

# We are IntechOpen, the world's leading publisher of Open Access books Built by scientists, for scientists

6,900

Open access books available

186,000

International authors and editors

200M

Downloads

Our authors are among the

154

Countries delivered to

TOP 1%

most cited scientists

12.2%

Contributors from top 500 universities



WEB OF SCIENCE™

Selection of our books indexed in the Book Citation Index  
in Web of Science™ Core Collection (BKCI)

Interested in publishing with us?  
Contact [book.department@intechopen.com](mailto:book.department@intechopen.com)

Numbers displayed above are based on latest data collected.  
For more information visit [www.intechopen.com](http://www.intechopen.com)



---

# Fatigue Fracture of Functionally Graded Materials Under Elastic-Plastic Loading Conditions Using Extended Finite Element Method

---

Somnath Bhattacharya, Kamal Sharma and Vaibhav Sonkar

Additional information is available at the end of the chapter

<http://dx.doi.org/10.5772/intechopen.72778>

---

## Abstract

In this chapter, extended finite element method (XFEM) has been used to simulate the fatigue crack growth problems in functionally graded material (FGM) in the presence of hole, inclusion and minor crack under elastic and plastic conditions. The fatigue crack growth analysis of alloy/ceramic FGMs, alloy and equivalent composite is done by XFEM in the presence of multiple discontinuities under mode-I mechanical load. The validity of linear elastic fracture mechanics (LEFM) theory is limited to the brittle materials. Therefore, the elastic plastic fracture mechanics (EPFM) theory needs to be utilized to characterize the plastic behavior of the material. A generalized Ramberg-Osgood material model has been used to model the stress-strain behavior of the material. Plasticity has been checked by Von Mises Yield criteria. J-integral has been used to calculate the SIF. Crack growth direction is determined by maximum principal stress criteria.

**Keywords:** FGM, composite materials XFEM, elastic-plastic loading, fatigue fracture, crack propagation, discontinuities, inclusions, holes, minor cracks

---

## 1. Introduction

Development of novel materials improves performance and efficiency of the structures, and also leads to development of advanced and sophisticated structures. This complex process of materials, structures and technology has led to the development of composite materials. Strength and stiffness plays a key role in evaluating the worth of the material. These characteristics provide strength to the structure to retain its desired shape and size under loading or any other external action.

---

Cracks/flaws are inevitable in all engineering materials. Loading under severe environmental conditions may either initiate new cracks or may cause the propagation of pre-existing cracks in the structures. Theoretically, fracture can be defined as the breaking or rupturing of a material resulting into its separation into two or more pieces.

Composite materials manifested in the middle of the twentieth century. Composites are naturally occurring or engineered materials made from two or more constituents with different chemical or physical properties distinct boundary among constituents. Lightweight composite materials with high strength to weight and stiffness to weight ratios have been used successfully in aircraft industry and other engineering applications. Under high temperature conditions the strength of the metal is deteriorated whereas, ceramics have excellent resistance to heat.

FGMs can be referred as multiphase composite materials in which the composition or microstructure or both are spatially varied which lead to a certain gradation in the local material properties. FGMs can be defined as multi-phase composites. FGMs are synthesized such that they own continuous variations in volume fractions of their components in space to return a pre-established composition. FGMs possess continuously varying properties in one or more than one direction and the form non-homogeneous macrostructure due to these variations. By gradually varying the volume fraction of the constituents, FGMs exhibit a smooth and continuous change from one surface to another, thus reducing interface problems, and minimizing thermal stress concentrations. The ceramic phase of FGMs provides a good resistance to heat, while the metal phase provides a strong mechanical performance and hence reduces the possibility of catastrophic failure.

The major advantages of FGM over conventional materials are firstly, FGM satisfies the working conditions for which it is specifically developed. Secondly, it is economical as it reduces material costs for particular engineering applications. Thirdly, it can reduce the magnitude of residual and thermal stresses generated under working conditions. Finally, FGMs exhibit better fracture toughness and bond strength. This is normally achieved by using a ceramic layer connected with a metallic layer. FGMs have wide area of engineering applications like in the computer circuit and aerospace industries. FGMs have typical applications is in aircraft and automotive industries as thermal barrier coatings (TBCs).

In general, all structural components are subjected to thermo-mechanical cyclic load. The fatigue life of these components is generally predicted without considering the effect of defects/discontinuities present in component. However, FGMs are commonly made by sintering process, which are porous in nature. These discontinuities at the vicinity of a major crack tip lead to increase the effective SIF at the major crack tip due to which the life of the components get depreciated. Hence, the analysis of FGMs in the vicinity of discontinuities becomes very important from the design point of view. To widen the spectrum of applications of FGMs, the fatigue/fracture behavior should be properly evaluated.

Over the years, greater understanding of fracture mechanics has undoubtedly prevented a significant number of structural failures. Fracture mechanics approach for the design of structures includes flaw size as one of the key variables. Fracture toughness replaces strength of material as a relevant material attribute, and its evaluation is mainly done in composites using the  $J$ -integral approach [1]. Failure of FGM has always been a trending domain of research for scientists and engineers due to the wide spectra of their engineering applications.

Fatigue and quasi-static fracture are two forms of crack growth phenomenon. Fatigue fracture refers to the slow propagation of cracks under cyclic loading conditions where the stress intensity factors are below the fracture toughness of the material. Quasi-static fracture is observed near the end of the fatigue life when the increased crack length leads to stress intensity factors which are above the fracture toughness [2, 3].

In many cases, multiple cracks may exist in the components. Their interaction resulting in the variation of stress intensity factor, stress distribution and propagation direction of the major crack. In the past, the failure of structures was analyzed in the presence of multiple cracks [4]. Some efforts have been made using analytical, experimental and simulation techniques to analyze the effect of interaction among multiple cracks [5–7].

Although, many analytical [8, 9] and experimental methods [10, 11] have been explored for the calculation of fracture parameters even then the drawbacks associated with experimental investigation and scarcity of analytical solution have impelled the analysts towards alternative techniques. Numerical methods hold the promise in this regard.

Many numerical methods are available to simulate the problems of fatigue failure in materials. These include finite element method (FEM), boundary element method, hybrid boundary node method [12, 13], meshfree methods [14–18] and extended finite element method [19, 20]. Out of these methods, FEM has been widely used for solving a wide variety of engineering and industrial problems [21–26]. It has achieved a remarkable success in solving various linear and non-linear problems [27–34]. Despite its numerous advantages and unparalleled success, it is not well-suited for solving the problems involving crack propagation. In crack growth problems, element edges provide natural lines along which a crack can grow. This is advantageous if the crack path is known a priori, but in most of the fracture phenomenon, the crack path is unknown. Thus, FEM requires a conformal mesh and re-meshing to ensure that the element boundaries coincide with the moving discontinuities (crack). Moreover, crack tip singularity cannot be accurately modeled by standard finite element approximation. Therefore, the modeling of crack growth becomes quite tedious and time consuming due to the modification in mesh topology at each stage of crack propagation. To overcome this difficulty, a new method known as extended finite element method (XFEM) has been developed to model arbitrary discontinuities without a need of conformal mesh or re-meshing. Level set method (LSM) is used in conjunction with XFEM for defining as well as tracking the geometry of cracks and other discontinuities like holes and inclusions. To cope up with these problems, XFEM has been adopted as a tool for the analysis of fatigue crack propagation in FGM.

## 2. Calculation of SIF for FGM

A domain based interaction integral approach can be used for calculating the stress intensity factors for homogeneous, bi-layer and functionally graded materials under thermal as well as mechanical loading. In this chapter, interaction integral approach will be extended to calculate the SIFs for FGM and bi-layered FGM under mechanical loads. The interaction integral is calculated based on  $J$ -integral. The  $J$ -integral for an elastic body subjected to thermo-mechanical load is given as,

$$J = \oint_{\Gamma_0} \left( \tilde{W} \delta_{1j} - \sigma_{ij} \frac{\partial u_i}{\partial x_1} \right) n_j d\Gamma \quad (1)$$

For the interaction integral calculation of an elastic body, consider two equilibrium states i.e. state 1, the actual state with given boundary conditions and state 2, an auxiliary state of the cracked body. The parameters for auxiliary state are represented with superscript  $a$ . The final expression for the interaction integral takes the form [35]

$$M_{12} = \int_{A_0} \left( \sigma_{ij} \frac{\partial u_i^a}{\partial x_1} + \sigma_{ij}^a \frac{\partial u_i}{\partial x_1} - \sigma_{ik}^a \varepsilon_{ik}^m \delta_{1j} \right) \frac{\partial q}{\partial x_j} dA + \int_{A_0} \left( \sigma_{ij} (S_{ijkl}^{tip} - S_{ijkl}(\mathbf{x})) \frac{\partial \sigma_{kl}^a}{\partial x_1} \right) q dA \quad (2)$$

where, the auxiliary field for the FGM may be taken from [36] as.

$$\sigma_{ij}^a = C_{ijkl}^{tip} \frac{1}{2} \left( \frac{\partial u_k^a}{\partial x_l} + \frac{\partial u_l^a}{\partial x_k} \right), \varepsilon_{ij}^a = S_{ijkl}(\mathbf{x}) \sigma_{kl}^a \quad \text{and} \quad \varepsilon_{ij}^a \neq \frac{1}{2} \left( \frac{\partial u_i^a}{\partial x_j} + \frac{\partial u_j^a}{\partial x_i} \right) \quad (3)$$

The SIFs are calculated from the interaction integral as [36]:

Mode-I SIF is given as,

$$K_I = \frac{M_{12} E^* \cosh^2(\pi \varepsilon^{tip})}{2} \quad \text{with} \quad K_I^a = 1 \quad \text{and} \quad K_{II}^a = 0 \quad (4a)$$

Mode-II SIF is given as,

$$K_{II} = \frac{M_{12} E^* \cosh^2(\pi \varepsilon^{tip})}{2} \quad \text{with} \quad K_I^a = 0 \quad \text{and} \quad K_{II}^a = 1 \quad (4b)$$

where,  $E^* = \frac{2\bar{E}_1 \bar{E}_2}{\bar{E}_1 + \bar{E}_2}$  with  $\bar{E}_i = \begin{cases} E_i^{tip} & \text{for plane stress} \\ E_i^{tip} / (1 - (\nu_i^{tip})^2) & \text{for plane strain} \end{cases}$  with  $i = 1, 2$

### 3. Fatigue crack growth

Here we use Paris law for stable crack propagation, the generalized Paris's law is given as:

$$\frac{da}{dN} = C(\Delta K_{Ieq})^m \quad (5)$$

Where,  $a$  is the crack length and  $N$  is the number of loading cycles.  $C$  and  $m$  are material properties to find the rate of crack growth. At each crack tip, the local direction of crack growth  $\theta_c$  can be calculated by the maximum principal stress theory [37]. Crack is assumed to grow in a direction perpendicular to the maximum principal stress. Thus, by enforcing the condition that the local shear stress is zero for  $\theta = \theta_c$ ,

$$K_I \sin \theta_c + K_{II} (3 \cos \theta_c - 1) = 0 \quad (6)$$

The solution of Eq. (6) gives

$$\theta_c = 2 \tan^{-1} \left( \frac{K_I - \sqrt{K_I^2 + 8K_{II}^2}}{4K_{II}} \right) \quad (7)$$

According to this criterion, the equivalent mode-I SIF is obtained as

$$K_{Ieq} = K_I \cos^3 \left( \frac{\theta_c}{2} \right) - 3K_{II} \cos^2 \left( \frac{\theta_c}{2} \right) \sin \left( \frac{\theta_c}{2} \right) \quad (8)$$

For stable crack propagation, the generalized Paris' law for FGM is given as

$$\frac{da}{dN} = C(x) (\Delta K_{Ieq})^{m(x)} \quad (9)$$

where,  $C(x)$  and  $m(x)$  are the functions of the location.

In the numerical example, the crack growth value  $\Delta a$  is assumed and the corresponding number of cycles  $\Delta N$  is computed from Eq. (9). When multiple crack tips are present, the crack growth value  $\Delta a$  is assumed for the most dominant crack tip, corresponding  $\Delta N$  is computed and then at the other crack tips the crack growth is computed corresponding to  $\Delta N$ . Eventually, when the maximum value of  $K_{Ieq}$  for any crack tip becomes more than the fracture toughness  $K_{IC}$  at corresponding location then the simulation is terminated. At this point, the total number of cycles elapsed is the fatigue life of the FGM.

#### 4. Modeling of the properties of FGM

In this chapter, the results have been presented for a FGM plate as shown in **Figure 1**. The FGM plate is manufactured by reinforcing an alloy with ceramic. The volume fraction of ceramic is varied in the  $x$ -direction to get a material property variation in the  $x$ -direction. It is assumed that at  $x = 0$  the FGM have the properties of the alloy and at  $x = L$  properties of ceramic. The major crack is always taken at the center of the FGM plate in the  $x$ -direction. The interface, when present is also in the same direction. The material properties of the aluminum alloy and alumina used in FGM are tabulated in **Table 1** [38, 39].

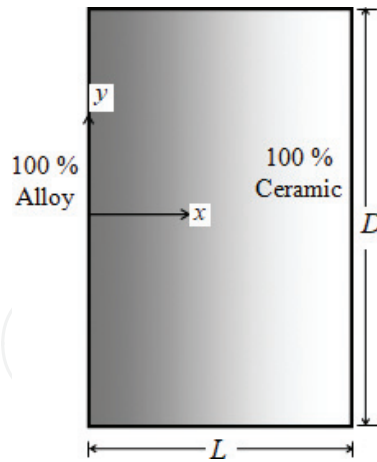


Figure 1. Geometry of the FGM plate along with its dimensions.

Material properties	Aluminum alloy	Alumina
Elastic modulus $E$ (GPa)	70	300
Poisson’s ratio, $\nu$	0.33	0.21
Coefficient of thermal expansion $\gamma$ ( $^{\circ}\text{C}$ )	$25 \times 10^{-6}$	$8.2 \times 10^{-6}$
Fracture toughness $K_{IC}$ (MPa $\sqrt{m}$ )	29	3.5
Paris law parameter $C$ in $m/cycle(\text{MPa}\sqrt{m})^{-m}$	$10^{-12}$	$2.8 \times 10^{-10}$
Paris law parameter, $m(x)$	3	10

Table 1. Material properties of aluminum alloy and alumina.

The variation of the elastic modulus for FGM is modeled as

$$E(x) = E_{alloy}e^{\alpha x} \text{ where } \alpha \text{ is given as } \alpha = \frac{1}{L} \ln\left(\frac{E_{ceramic}}{E_{alloy}}\right) \tag{10}$$

A plot of  $E(x)$  for  $L = 100$  mm is shown in **Figure 2**. The fatigue life of FGM has been compared with the same of the aluminum alloy and an equivalent composite of aluminum alloy/alumina. The equivalent composite considered in this example has the same overall volume fractions of aluminum alloy and ceramic as the FGM. The volume fractions of ceramic and aluminum alloy in the FGM are obtained as

$$V_{ceramic}^{FGM}(x) = \frac{E(x) - E_{alloy}}{E_{ceramic} - E_{alloy}} = \frac{E_{alloy}e^{\alpha x} - E_{alloy}}{E_{ceramic} - E_{alloy}} \tag{11a}$$

$$V_{alloy}^{FGM}(x) = 1 - V_{ceramic}^{FGM}(x) \tag{11b}$$

In this example, the equivalent composite is assumed to have the same amount of metal and ceramic. The volume fraction of alumina in the equivalent composite is calculated as

$$V_{ceramic}^{composite} = \frac{1}{L} \int_0^L V_{ceramic}^{FGM}(x) dx \quad (11c)$$

where,  $L$  is the length of the plate. For  $L = 100$  mm,  $V_{ceramic}^{composite} = 38.28\%$  and  $V_{alloy}^{composite} = 61.72\%$ . The variation in volume fraction of ceramic (alumina) in the FGM is shown in **Figure 3**. The volume fraction for the equivalent composite has also been indicated. Now, using the rule of mixtures for the equivalent composite

$$E_{composite} = E_{alloy} V_{alloy}^{composite} + E_{ceramic} V_{ceramic}^{composite} \quad (12)$$

we get  $E_{composite} = 158.04$  GPa. The Poisson's ratio for the equivalent composite as well as for the FGM may be calculated as [40]

$$\nu(x) = \frac{\nu_{alloy} V_{alloy}^{FGM}(x) E_{ceramic} + \nu_{ceramic} V_{ceramic}^{FGM}(x) E_{alloy}}{V_{alloy}^{FGM}(x) E_{ceramic} + V_{ceramic}^{FGM}(x) E_{alloy}} \quad (13a)$$

$$\text{and } \nu_{composite} = \frac{\nu_{alloy} V_{alloy}^{composite} E_{ceramic} + \nu_{ceramic} V_{ceramic}^{composite} E_{alloy}}{V_{alloy}^{composite} E_{ceramic} + V_{ceramic}^{composite} E_{alloy}} \quad (13b)$$

The Poisson's ratio is shown in **Figure 4**.

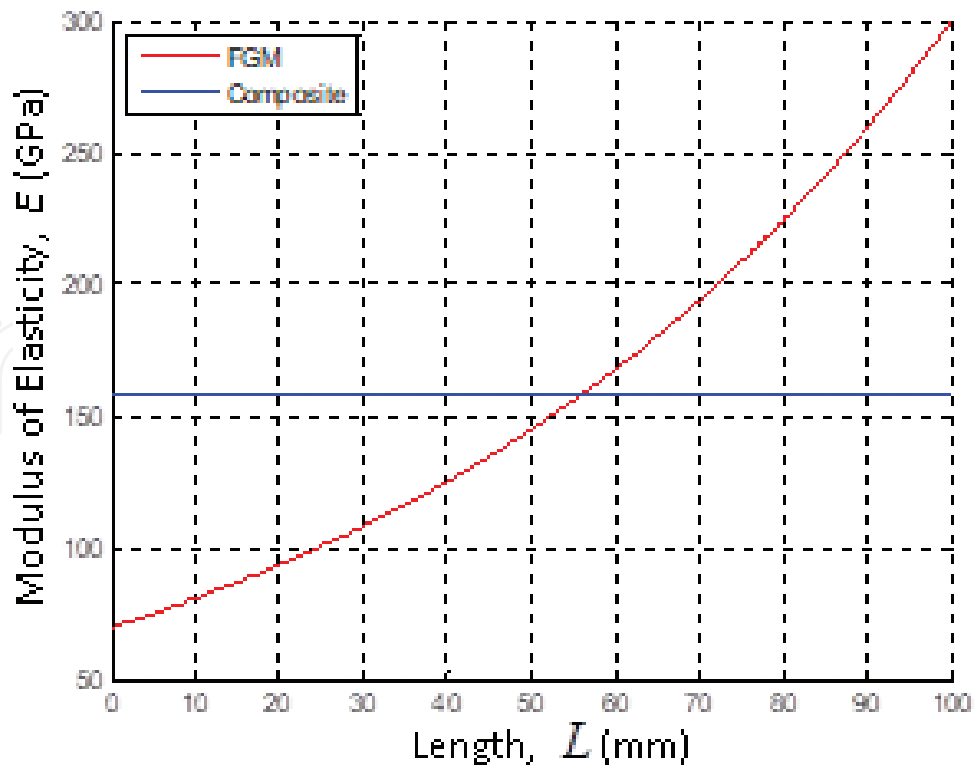


**Figure 2.** Variation of modulus of elasticity along the length of the plate.

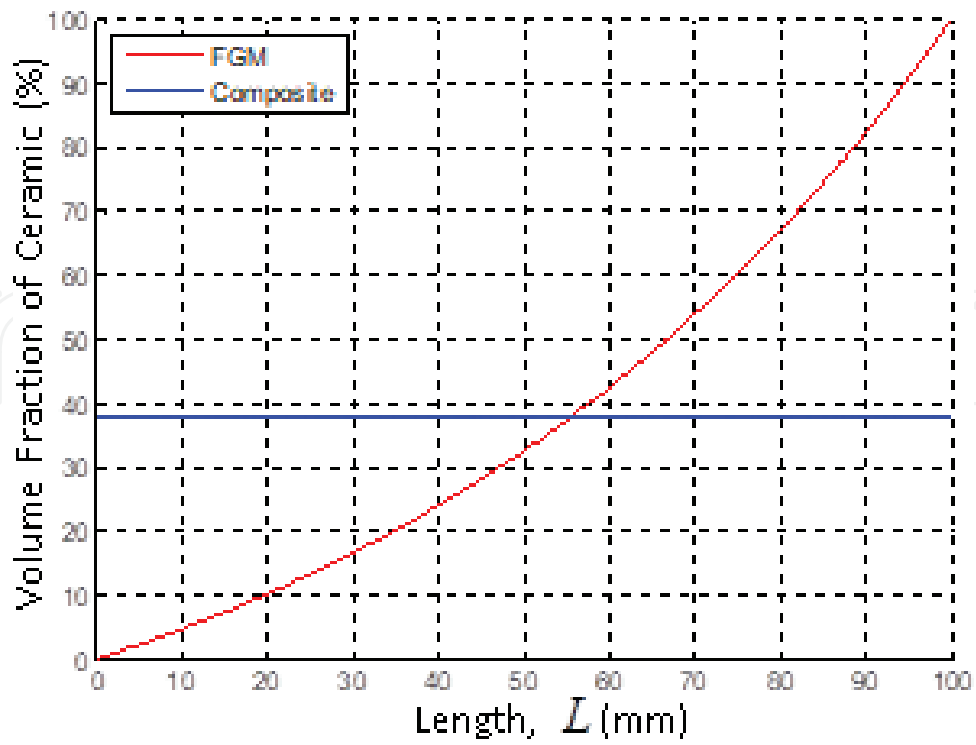


Figure 3. Variation of volume fraction of ceramic along the length of the plate.

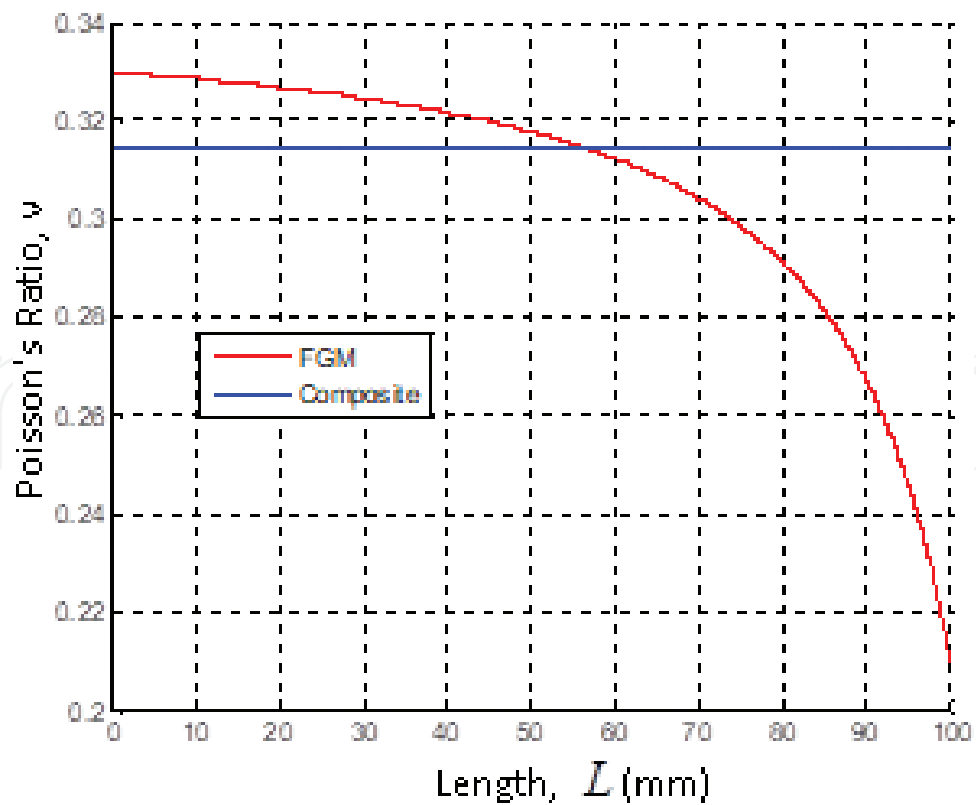


Figure 4. Variation of Poisson's ratio along the length of the plate.

The coefficient of thermal expansion for the FGM by the rule of mixtures is calculated as

$$\gamma(x) = \gamma_{alloy} V_{alloy}^{FGM}(x) + \gamma_{ceramic} V_{ceramic}^{FGM}(x) \quad (14a)$$

The coefficient of thermal expansion for the equivalent composite is given by

$$\gamma_{composite} = \gamma_{alloy} V_{alloy}^{composite} + \gamma_{ceramic} V_{ceramic}^{composite} \quad (14b)$$

The value of the coefficient of thermal expansion for the equivalent composite is calculated using Eq. (14b) and is found to be  $\gamma_{composite} = 18.57 \times 10^{-6}/^{\circ}\text{C}$ . A variation of coefficient of thermal expansion for the FGM is shown in **Figure 5**.

The fracture toughness of the FGM as well as the equivalent composite may be expressed as a function of the volume fraction of the ceramic by the following formula given by [41]

$$K_{IC}(x) = \frac{K_{IC}^{alloy} + K_{IC}^{ceramic}}{2} + \frac{K_{IC}^{alloy} - K_{IC}^{ceramic}}{2} \left( \sqrt{1 - V_{ceramic}^{FGM}(x)} - \sqrt{V_{ceramic}^{FGM}(x)} \right) \quad (15a)$$

$$K_{IC}^{composite} = \frac{K_{IC}^{alloy} + K_{IC}^{ceramic}}{2} + \frac{K_{IC}^{alloy} - K_{IC}^{ceramic}}{2} \left( \sqrt{1 - V_{ceramic}^{composite}} - \sqrt{V_{ceramic}^{composite}} \right) \quad (15b)$$

The variation of fracture toughness is shown in **Figure 6**.

The Paris law parameters are assumed to have exponential variation in a manner similar to the elastic modulus. Thus, the variation in the parameters of Paris equation is taken as

$$C(x) = C_{alloy} e^{\vartheta x}, \text{ where, } \vartheta = \frac{1}{L} \ln \left( \frac{C_{ceramic}}{C_{alloy}} \right) \quad (16)$$

$$m(x) = m_{alloy} e^{\zeta x}, \text{ where, } \zeta = \frac{1}{L} \ln \left( \frac{m_{ceramic}}{m_{alloy}} \right) \quad (17)$$

For the equivalent composite, we find the location at which the volume fraction of ceramic in the FGM is same as that of the equivalent composite. This location  $\bar{x}$  may be found by either **Figure 5** or by using the formula  $\bar{x} = \frac{1}{\alpha} \ln \left( \frac{E_{composite}}{E_{alloy}} \right)$ , where  $\alpha$  is defined in Eq. (10). For the present example  $\bar{x} = 56$  mm. The Paris law parameters of the equivalent composite is assumed to be same as that of the FGM at  $x = \bar{x}$ . Thus,

$$C_{composite} = C_{alloy} e^{\vartheta \bar{x}} \quad (18a)$$

$$m_{composite} = m_{alloy} e^{\zeta \bar{x}} \quad (18b)$$

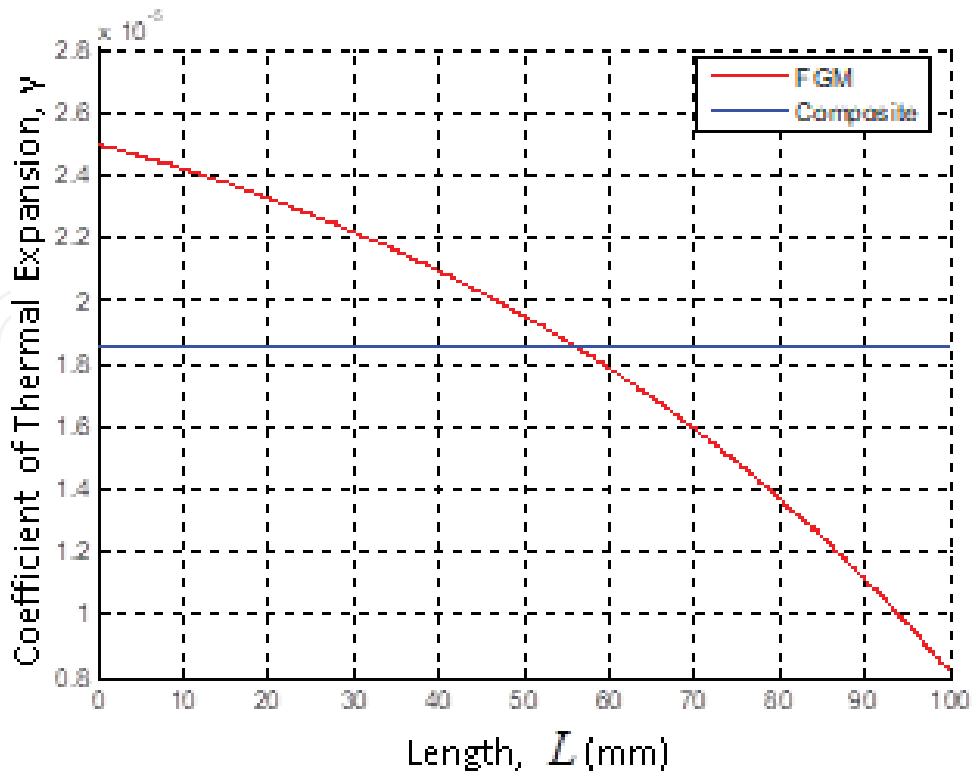


Figure 5. Variation of coefficient of thermal expansion along the length of the plate.

The values of  $C$  and  $m$  for the equivalent composite comes out to be  $C_{composite} = 2.34 \times 10^{-11} \text{ m/cycle (MPa}\sqrt{\text{m}})^{-m}$  and  $m_{composite} = 5.88$ . The variation of  $C$  and  $m$  are shown in **Figures 7 and 8** respectively.

Plastic behaviour for FGM can be modeled using Ramberg Osgood equation [42]

$$\varepsilon = \frac{\sigma}{E} + \left(\frac{\sigma}{H}\right)^{1/n} \quad (19)$$

Here,  $H$  is the strength coefficient and  $n$  is the strain hardening exponent. The value of  $n = 0.0946$  is used for the present example. The values of the parameters of Paris equation are taken as  $C = 3 \times 10^{-11}$  and  $m = 3$ . In actual case the path of crack growth is curved but in this study the linear crack growth path is taken. Linear crack extension length  $\Delta a$  for an edge crack is kept constant. For a center crack maximum crack extension length  $\Delta a_{max}$  is kept on principal crack tip. The principle crack tip is the crack tip where  $\Delta K_{Ieq}$  maximum. Crack increment at the other crack tip is given by:

$$\Delta a = \Delta a_{max} \left(\frac{\Delta K_{Ieq}}{\Delta K_{Ieq \max}}\right)^m \quad (20)$$

The crack tip extension at the principal crack tip is  $\Delta a_{max}$  and at the other crack tip extension is smaller. The crack extension takes place  $K_{Ieq \max} < K_{IC}$ . Crack becomes unstable when

$K_{Ieq\ max} > K_{IC}$ . Simulation continues until this condition is met. Here,  $K_{Ieq\ max}$  is the equivalent SIF for mode-I at principal crack tip and  $K_{IC}$  is the material property called fracture toughness or critical SIF.  $K_{IC}$  for FGM is given by [35]

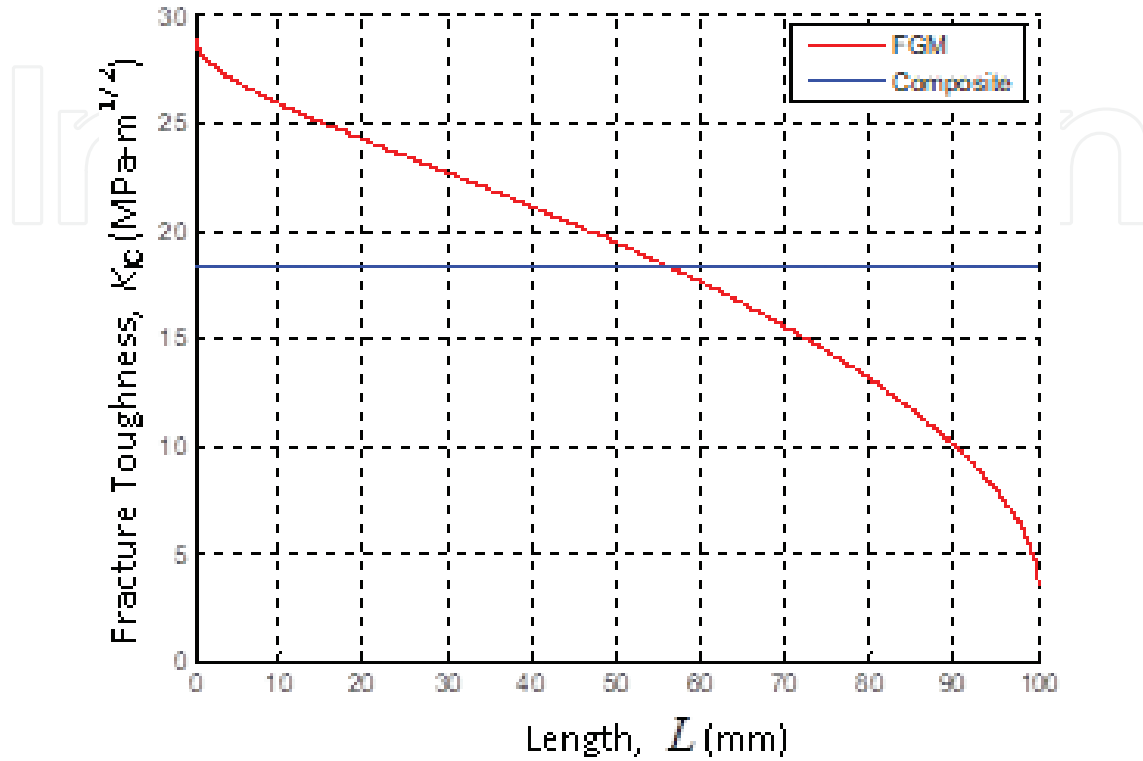


Figure 6. Variation of fracture toughness along the length of the plate.

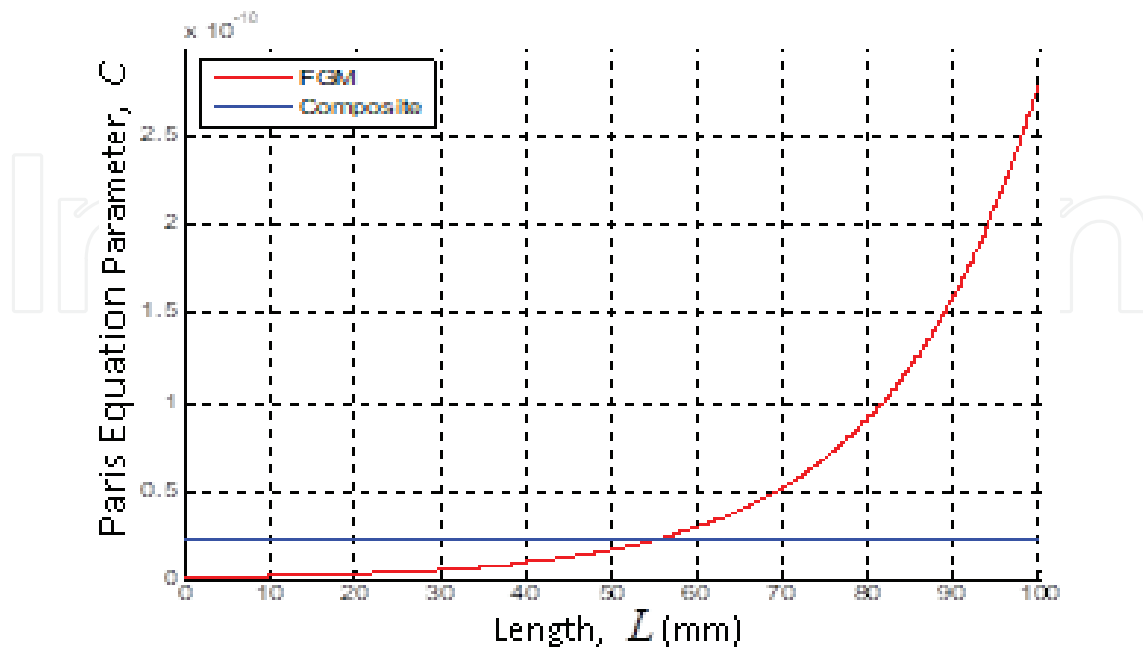


Figure 7. Variation of  $C(x)$  along the length of the plate.

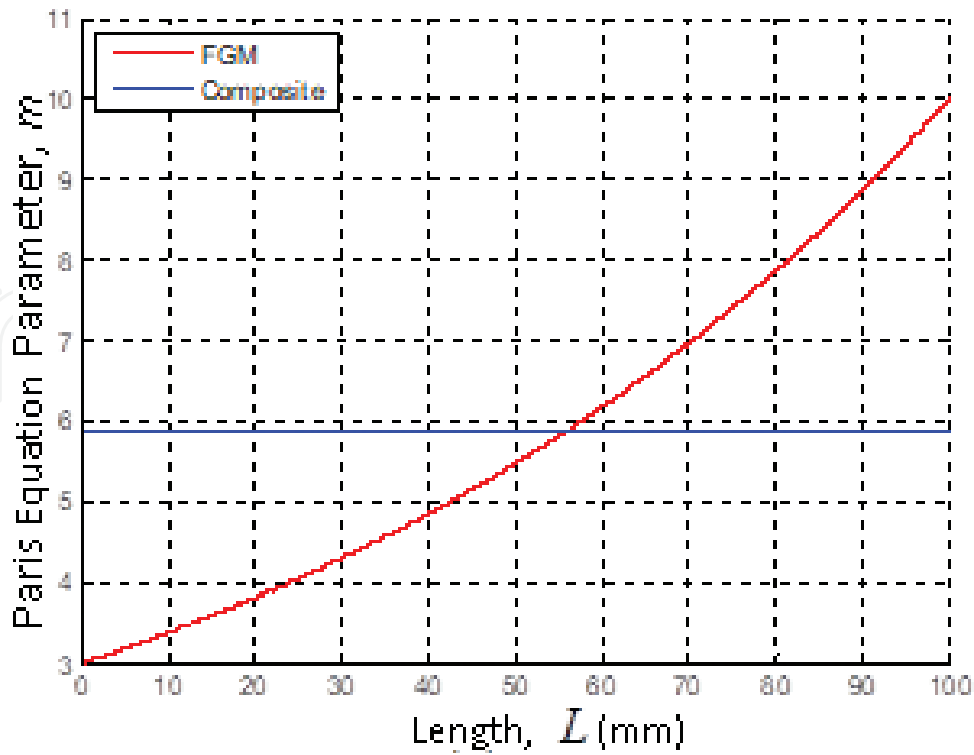


Figure 8. Variation of  $m(x)$  along the length of the plate.

$$K_{IC}(x) = K_{IC}^{ceramic} \left[ \frac{E(x)}{1 - \nu_{FGM}^2} \left\{ V_m(x) \frac{1 - \nu_{alloy}^2}{E_{alloy}} \left( \frac{K_{IC}^{alloy}}{K_{IC}^{ceramic}} \right)^2 + (1 - V_m(x)) \frac{1 - \nu_{ceramic}^2}{E_{ceramic}} \right\} \right]^{1/2} \quad (21)$$

where  $K_{IC}(x)$  is the fracture toughness of the FGM at point  $x$ .  $K_{IC}^{alloy}$  and  $K_{IC}^{ceramic}$  are the fracture toughness of the alloy and ceramic, while  $\nu_{alloy}$  and  $\nu_{ceramic}$  are Poisson’s ratios for the alloy and ceramic respectively.  $V_m(x)$  denotes the volume fraction for the alloy at point  $x$ .

The constitutive relation for the elastic-plastic material is given as

$$\sigma(u) = D_{ep}(x)\varepsilon(u) \quad (22)$$

where  $x$  is the vector of  $x$  and  $y$ -coordinates,  $D_{ep}(x)$  is elastic-plastic constitutive matrix varying in  $x$ -direction. The elastic constitutive matrix can be written for plane stress condition as

$$D_e(x) = \frac{E(x)}{\{1 - \nu(x)^2\}} \begin{bmatrix} 1 & \nu(x) & 0 \\ \nu(x) & 1 & 0 \\ 0 & 0 & \frac{1 - \nu(x)}{2} \end{bmatrix} = D \quad (23a)$$

and for plane strain condition as

$$D_e(\mathbf{x}) = \frac{E(\mathbf{x})}{\{1 - 2\nu(\mathbf{x})\}\{1 + \nu(\mathbf{x})\}} \begin{bmatrix} 1 - \nu(\mathbf{x}) & \nu(\mathbf{x}) & 0 \\ \nu(\mathbf{x}) & 1 - \nu(\mathbf{x}) & 0 \\ 0 & 0 & \frac{1 - 2\nu(\mathbf{x})}{2} \end{bmatrix} = D \quad (23b)$$

The incremental theory of plasticity [43] has been used to model the elastic-plastic constitutive relation for a material. An incremental stress vector  $d\sigma$  and incremental strain vector  $d\varepsilon$  are such that  $d\sigma = D_{ep}.d\varepsilon$ . Where  $D_{ep}$  is the elastic-plastic constitutive matrix, which is determined as discussed under:

Total strain increment is the sum of elastic and plastic strains

$$d\varepsilon = d\varepsilon_e + d\varepsilon_p \quad (24)$$

Elastic incremental strain and stress is determined

$$d\sigma = D_e d\varepsilon_e \quad (25)$$

$$F(\sigma) = f(\bar{\sigma}) \quad (26)$$

where  $\sigma$  is the stress tensor and  $\bar{\sigma}$  is the equivalent stress,  $F$  and  $f$  are two different failure functions. By the flow rule the incremental strain is related to the gradient of a function known plastic potential. If the plastic potential function and the failure function is same, then the following relation is obtained,

$$d\varepsilon_p = \nabla F.d \lambda \quad (27)$$

Plastic modulus  $H$  is given as

$$H = \frac{d\bar{\sigma}}{d\bar{\varepsilon}_p} \quad (28)$$

For a given strain energy  $\delta w$ , and according to the definition of  $d\varepsilon_p$  we must have,

$$\delta w = \bar{\sigma}.d\bar{\varepsilon}_p \quad (29)$$

According to the Von Mises criteria,  $F = J_2$ , where  $J_2$  is the second invariant of deviatoric stress tensor. So, we must have  $F(\bar{\sigma}) = \frac{\bar{\sigma}^2}{3}$ , Thus Eqs. (26) and (27) result in

$$d\sigma = D_e \{d\varepsilon - d\varepsilon_p\} \quad (30)$$

After taking the derivatives from both sides of failure criteria equation

$$\left(\frac{\partial F}{\partial \sigma} d\sigma\right) = \left(\frac{\partial f}{\partial \bar{\sigma}} \cdot \frac{\partial \bar{\sigma}}{\partial \bar{\varepsilon}_p} \cdot \frac{\partial \bar{\varepsilon}_p}{\partial w} \cdot \frac{\partial w}{\partial \bar{\varepsilon}_p} \cdot d\varepsilon_p\right) \quad (31)$$

For simplicity we take  $\frac{\partial F}{\partial \sigma} = a$ ,  $\frac{\partial f}{\partial \bar{\sigma}} = \bar{a}$

$$a.d\sigma = \bar{a}.H.\left(\frac{1}{\sigma}\right)\sigma.d\varepsilon_p \quad (32)$$

$d\lambda$  is calculated by omitting  $d\sigma$  between Eqs. (30) and (31) and substituting  $d\varepsilon_p$  from Eq. (27). By substituting  $d\lambda$  in Eq. (27), the final form of material matrix is obtained as [43]

$$D_{ep} = D_e - D_p \quad (33)$$

$$\text{where } D_p = \frac{Da a^T D}{\frac{a}{\sigma} H \sigma^T + a^T D a} \quad (34)$$

## 5. XFEM: Introduction and formulation for cracks and discontinuities in FGM

XFEM or the extended finite element method is a numerical technique which allows crack modeling irrespective of the mesh, and eliminates the cumbersome process of remeshing in problems involving change in the crack geometry like crack growth. XFEM models a crack by enriching the standard finite element approximation with some functions, which are obtained from the theoretical background of the problem. Moving discontinuities are tracked by the level set method. XFEM is a numerical method, based on the finite element method (FEM) that is especially designed for treating discontinuities. The formulation is done as discussed in [35, 44]. The solution of FGM differs from homogeneous materials only in the spatial gradation in the material properties. After calculating the values of stress and strain, the SIF is determined.

## 6. Numerical examples and discussion

The FGM plate considered in all the numerical simulations has 100% aluminum alloy on one side and 100% alumina on the other side. The volume fraction of alumina changes from 0% on one side to 100% on the other side so as to produce an FGM. The equivalent composite is equivalent to the FGM in the sense that both the FGM and the composite plate contain the same amount of aluminum alloy and alumina. The fatigue crack growth analysis of alloy/ceramic FGMs, aluminum alloy and equivalent composite is done by XFEM in the presence of multiple cracks, holes and inclusions under mode-I mechanical load and their fatigue life are compared. The constituents of the FGM plate are aluminum alloy and alumina. A major crack of large initial length is assumed to exist at the edge of the plate. The major crack is assumed to be in the direction of material gradation. The fatigue crack growth analyses of the FGM, the equivalent composite and the aluminum alloy plates have been carried out in the presence of minor cracks, holes and inclusions till the final failure of the plate under mode-I mechanical load. The effect of these small defects on the fatigue life as well as on the crack path has been investigated in detail.

### 6.1. Example 1

A rectangular FGM plate of length ( $L$ ) 100 mm. and height ( $D$ ) 200 mm. with 100% aluminum alloy on left side and 100% ceramic (alumina) on right side is considered. Property variation is taken in  $x$ -direction, where  $x = 0$  to  $x = 100$  mm. The plate with a major edge crack of length  $a = 20$  mm is analyzed under plane strain condition in the presence of multiple discontinuities. In all simulations, the plate dimensions, initial crack length and material properties are taken to be same. The properties of FGM, composites and aluminum alloy are already described in **Table 1**. The material properties of the inclusions are taken as  $E = 20$  GPa and  $\nu = 0.2$ . The plate domain is discretized using uniformly distributed 117 nodes in  $x$ -direction and 235 nodes in  $y$ -direction. The fatigue crack growth analysis is performed by taking a crack increment of  $\Delta a = \frac{a}{10} = 2$  mm. A cyclic tensile load varying from  $\sigma_{\max} = 70$  MPa to  $\sigma_{\min} = 0$  MPa is applied in all the simulations. The geometric discontinuities like holes, inclusions and minor cracks are added in the plate in addition to the major edge or center crack to analyze their effect on the fatigue life of the material. The fatigue life of the FGM, equivalent composite and aluminum alloy are obtained under mode-I loading, and are compared with each other.

### 6.2. Plate with a major edge crack under linear elastic condition

**Figures 9** and **10** show a plate with a major edge crack of length  $a = 20$  mm at the left and right edge respectively. These plates have been analyzed under plane strain condition using a uniform mesh of 117 by 235 nodes. The plots of the fatigue life for different materials are shown in **Figure 11**. From these figures, it is seen that the equivalent composite withstands 7885 cycles before it fails while the FGM with crack on alloy side undergoes 15,561 cycles and

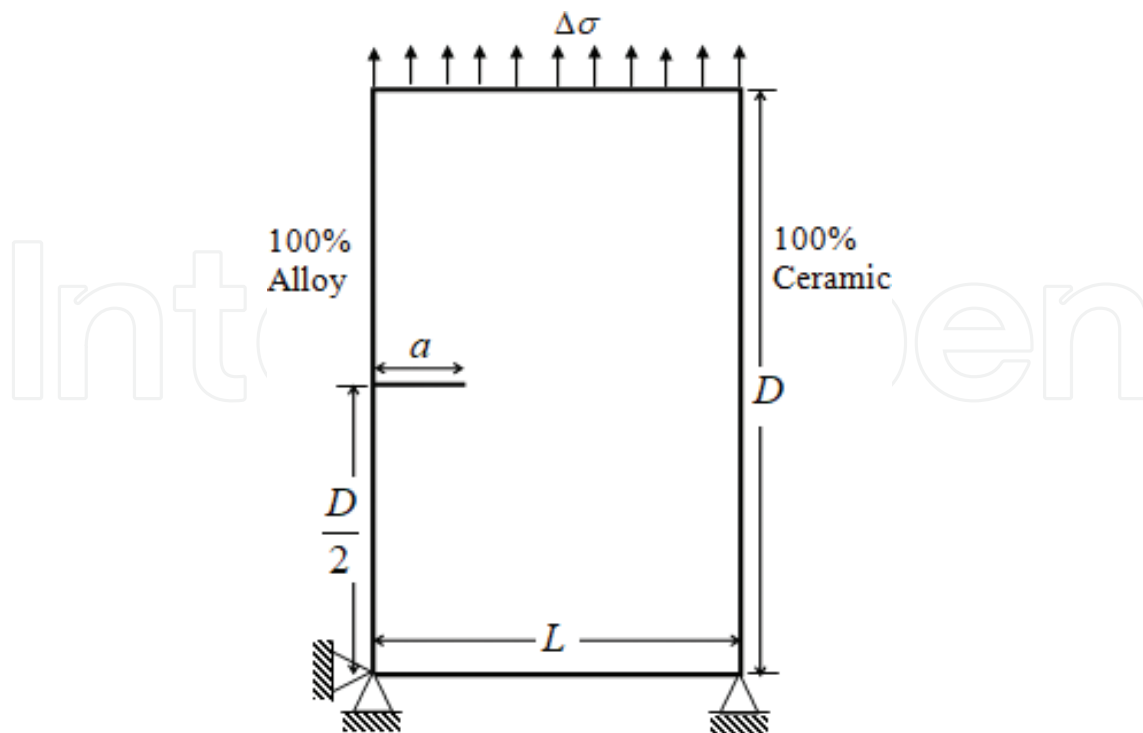


**Figure 9.** Plate with an edge crack on the alloy rich side under mode-I loading.

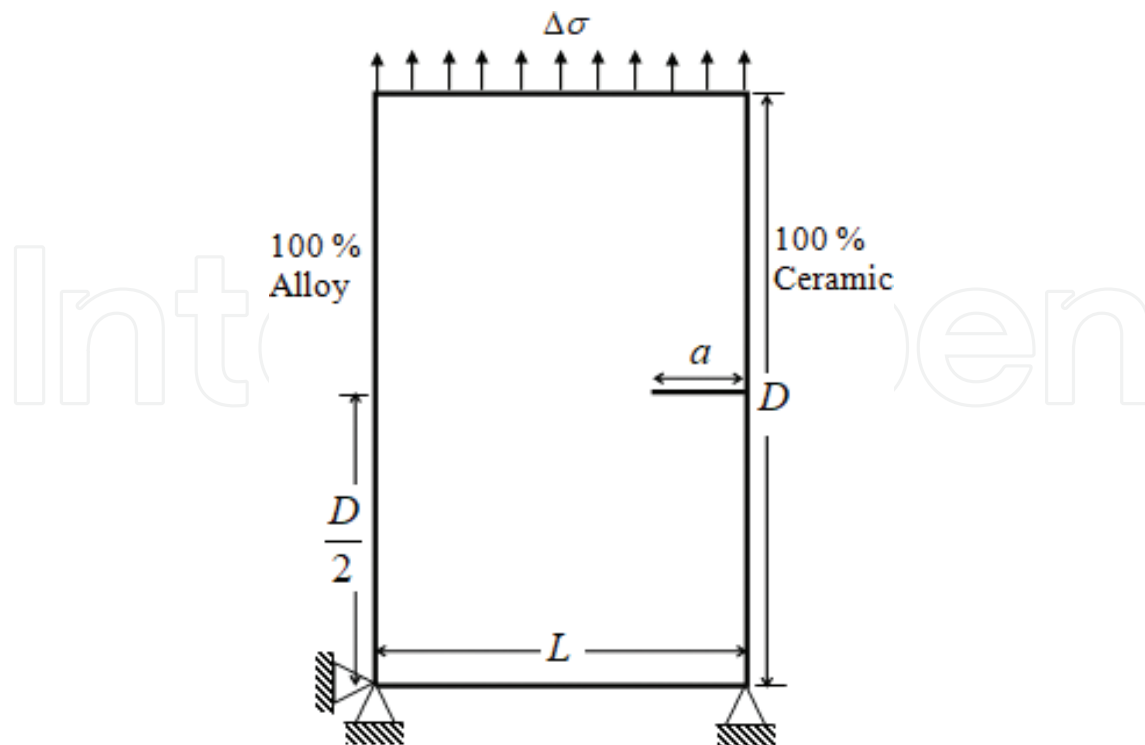


**Figure 10.** Plate with an edge crack on the ceramic rich side under mode-I loading.

pure aluminum alloy undergoes 19,145 cycles before failure. It is also observed that when a major crack initiates from the ceramic (alumina) rich side then it fails much earlier (4872 cycles) as compared to when the crack initiates from the aluminum alloy side.

These plots show that when a crack is present on the ceramic rich side, the life diminishes by a considerable extent as compared to when a crack is present on the alloy rich side. The equivalent composite shows the minimum life except in case when a crack is present on the ceramic side. It is also observed that the crack follows nearly a straight path in all the materials.

### 6.3. Plate with a major edge crack, minor cracks, holes and inclusions under linear elastic condition

In this case, a major crack of length  $a = 20$  mm. is taken at the left and the right edge of the plate ( $100 \times 200$  mm) as shown in **Figures 12** and **13** respectively. In addition to the major edge crack, 36 minor cracks, 15 holes and 15 inclusions are randomly distributed in the plate. The length of the minor cracks varies from 3.5 to 4.5 mm, and orientation varies from  $0$  to  $60^\circ$  randomly. The holes and inclusions have variations in their radii from 3 to 4.5 mm randomly. A cyclic mode-I mechanical load is applied at the top edge of the plate. The plots for crack extension with number of cycles are shown in **Figure 14**.

It is also observed that the crack deflects in all the materials. Moreover, it is seen that the number of cycles to failure in case of aluminum alloy is about 18,111 cycles whereas in case of FGM with crack on the alloy and ceramic rich sides is 14,622 cycles and 3111 cycles respectively. The fatigue life of the composite plate is found to 6956 cycles. Thus, it can be stated that

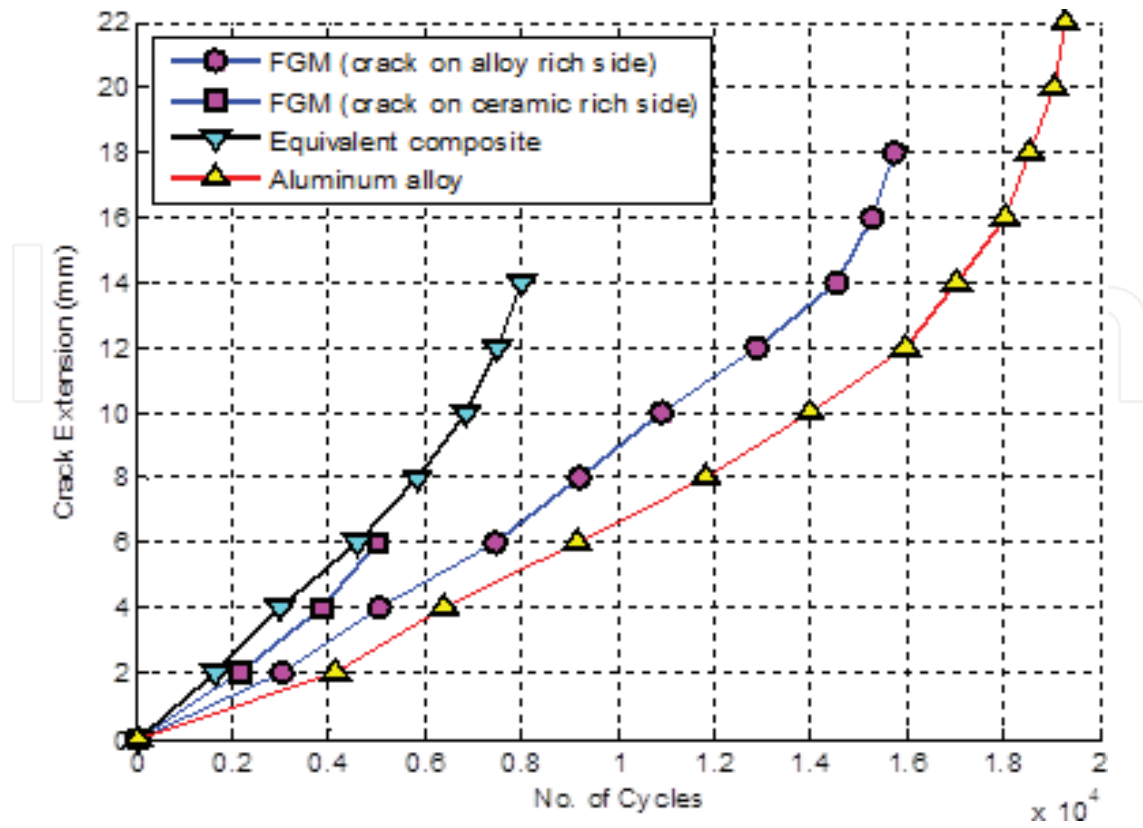


Figure 11. A plot of crack extension with number of cycles.

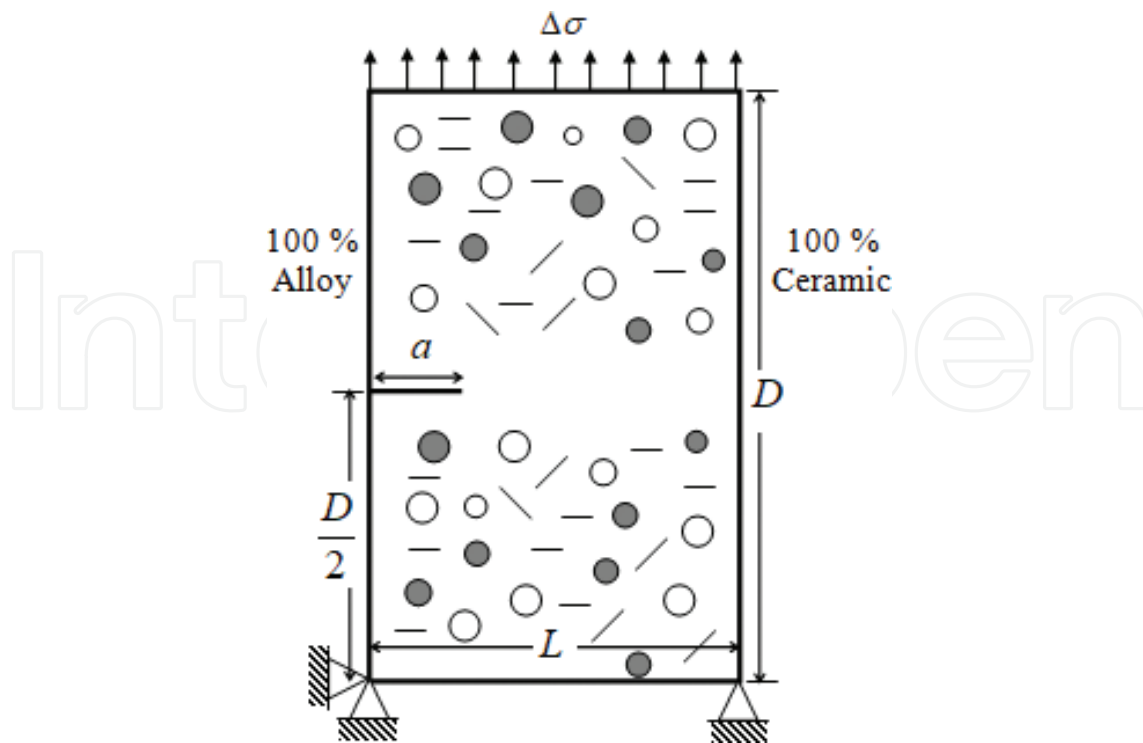


Figure 12. Plate with an edge crack on the alloy rich side under mode-I loading.

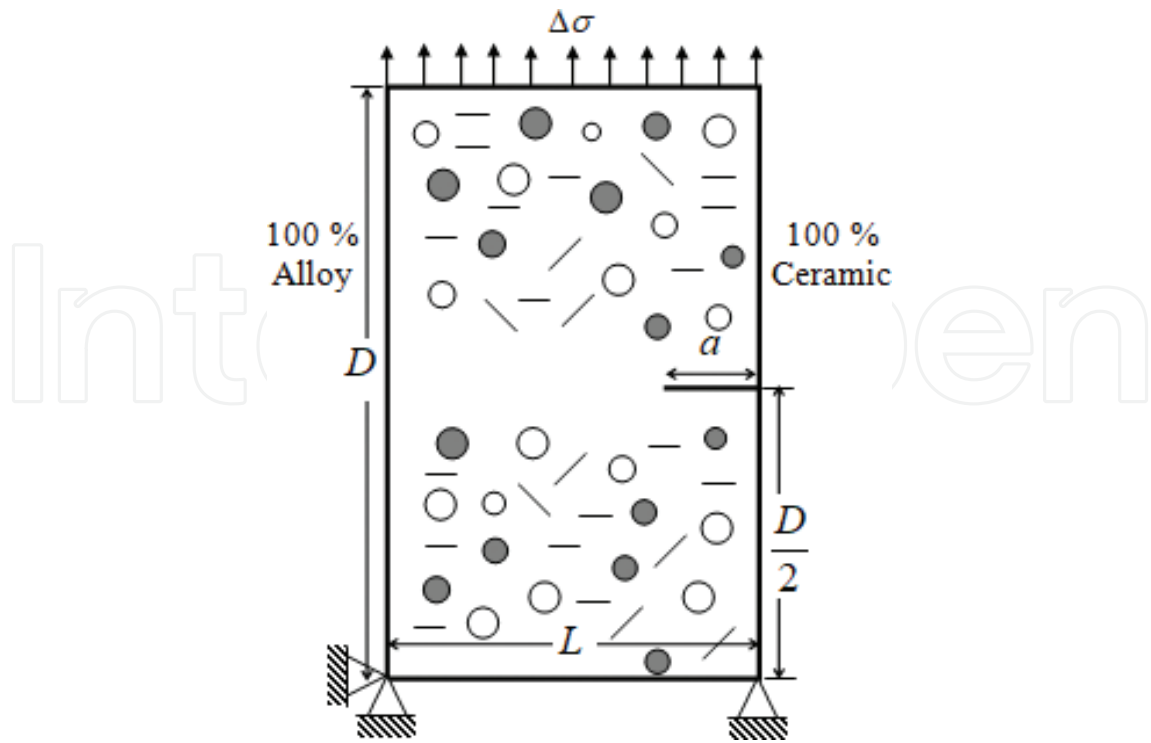


Figure 13. Plate with an edge crack on the ceramic rich side under mode-I loading.

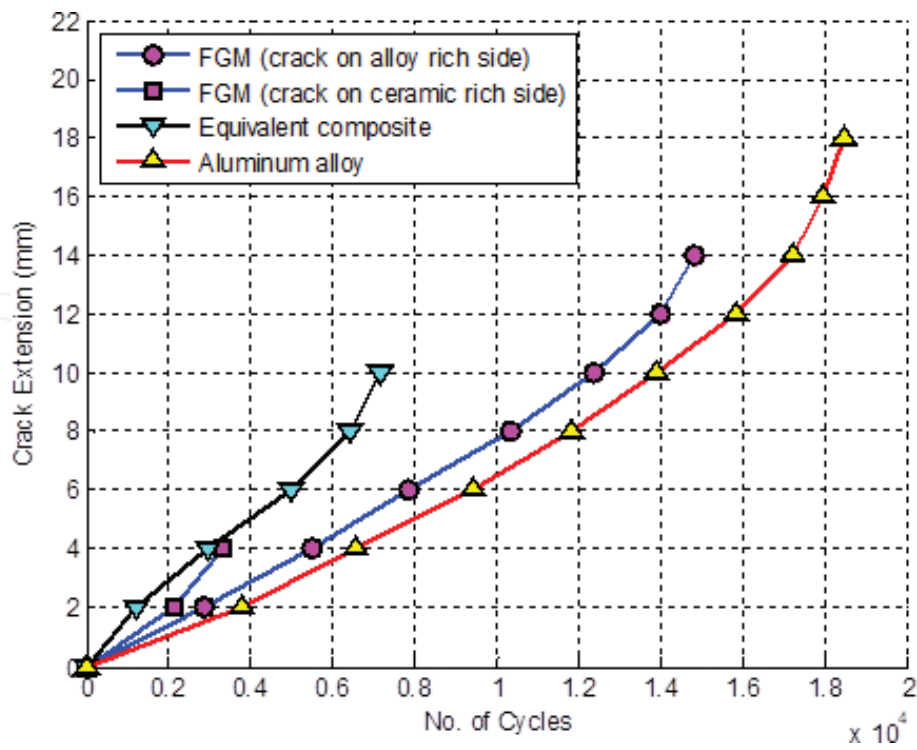


Figure 14. A plot of crack extension with number of cycles.

due to the presence of minor cracks, holes and inclusions, the life of the aluminum alloy is reduced by about 5.42%, whereas the fatigue life of the FGM with crack on the alloy and ceramic rich sides goes down by 6.03 and 36.15% respectively. The fatigue life of the equivalent composite is reduced by 11.78%.

#### 6.4. Example 2

A rectangular FGM plate of length ( $Lt$ ) 100 mm. and height ( $Ht$ ) 200 mm. with 100% copper nickel alloy on left side and 100% ceramic (alumina) on right side is considered. Property variation is taken in x-direction, where x varies from  $x = 0$  to  $x = 100$  mm. A uniform traction of 100 MPa is applied on the top edge of the rectangular domain along y direction. Cyclic loading is applied at top edge of the plate with a maximum value of  $\sigma_{max} = 100$  MPa and minimum value of  $\sigma_{min} = 0$  MPa. A uniform mesh of size  $117 \times 235$  nodes is used for the analysis in each case. The values of SIFs are computed at the tip of the major crack. The variation of SIF with crack length is plotted in each case. The material properties are taken from **Table 2** [43].

#### 6.5. A major crack in FGM plate under elastic: Plastic loading condition

In this case, a major crack of length  $a = 20$  mm is taken at the edge of the domain ( $100 \times 200$  mm) as shown in **Figure 15**. Cyclic loading is applied at the top edge of the FGM plate, and a crack propagates due to this loading. The plots of SIF with crack length for an crack configuration is shown in **Figure 16**. The failure crack length obtained for edge crack is 0.0402 m.

Material properties	Values
Elastic modulus of copper nickel alloy $E_{alloy}$ (GPa)	160
Elastic modulus of alumina (ceramic) $E_{ceramic}$ (GPa)	386
Elastic modulus of soft inclusion $E_{inclusion}$ (GPa)	100
Elastic modulus of Hard inclusion $E_{inclusion}$ (GPa)	400
Poisson's ratio of copper nickel alloy $\nu_{alloy}$	0.35
Poisson's ratio of alumina (ceramic) $\nu_{ceramic}$	0.21
Poisson's ratio of inclusion $\nu_{inclusion}$	0.3
Poisson's ratio of inclusion $\nu_{FGM}$	0.23
Fracture toughness of copper nickel alloy $K_{IC}^{alloy}$ (MPa $\sqrt{m}$ )	79
Fracture toughness of alumina (ceramic) $K_{IC}^{ceramic}$ (MPa $\sqrt{m}$ )	5
Paris constant C in $m/cycle(MPa\sqrt{m})^{-m}$	$3 \times 10^{-11}$
Paris exponent $m$	3

**Table 2.** Material property table.

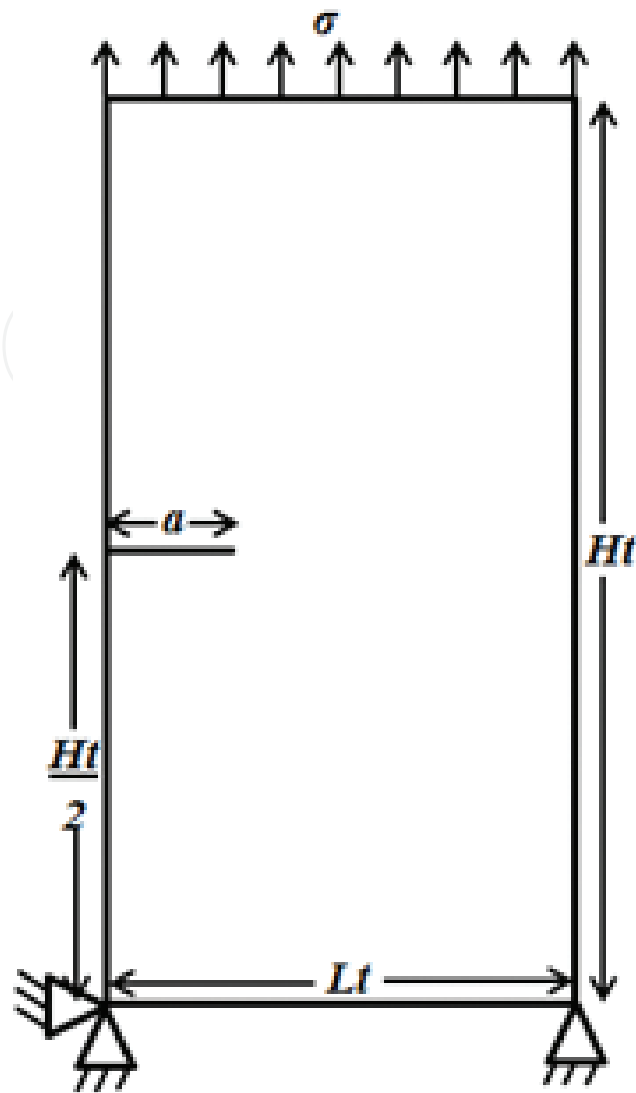


Figure 15. FGM plate with an edge crack.

### 6.6. A major edge crack in FGM plate with holes, inclusions and minor cracks under elastic-Plastic loading condition

In this case, a major crack of length  $a = 20$  mm is taken at the edge of the domain ( $100 \times 200$  mm) is taken as shown in **Figure 17**. Minor cracks, holes and inclusions are randomly distributed in the plate. All 36 minor cracks have varying length randomly from 3.5 to 4.5 mm, with varying orientation from  $0$  to  $60^\circ$ . In addition to these 15 inclusions are also distributed in the domain randomly. The holes and inclusions have variation in their radii from 3 to 4.5 mm. A cyclic mode-I loading is applied due to which the major crack propagates. The plots for SIF variation with crack length of edge crack is shown in **Figures 18** and **19** for soft and hard inclusions respectively. The failure crack length for edge crack is obtained 0.0384 and 0.0392 m. for soft and hard inclusions respectively.

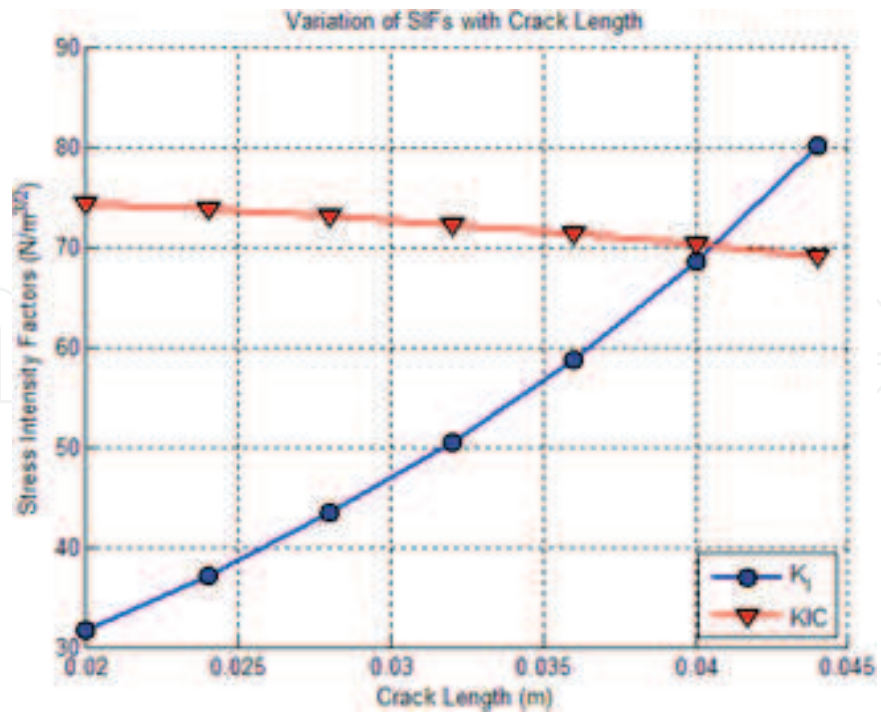


Figure 16. Plot for variation of SIF with crack length.

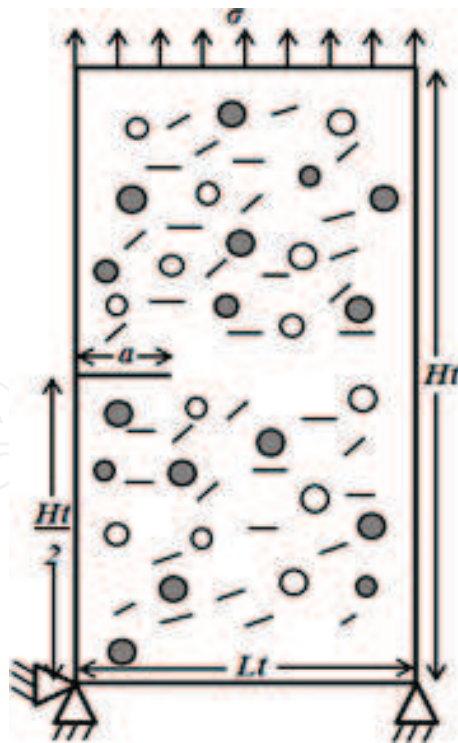


Figure 17. FGM plate with an edge crack, 15 inclusions, 15 holes and 36 minor cracks.

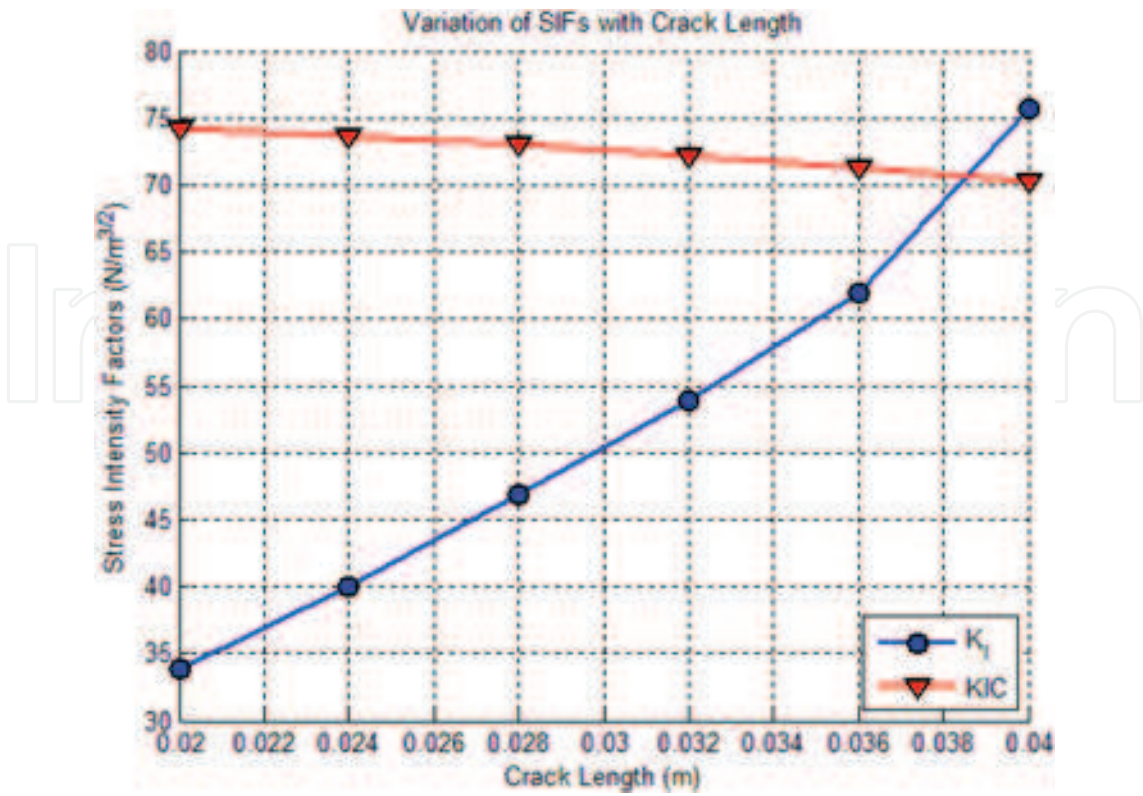


Figure 18. Plot for variation of SIF with crack length for soft inclusions.

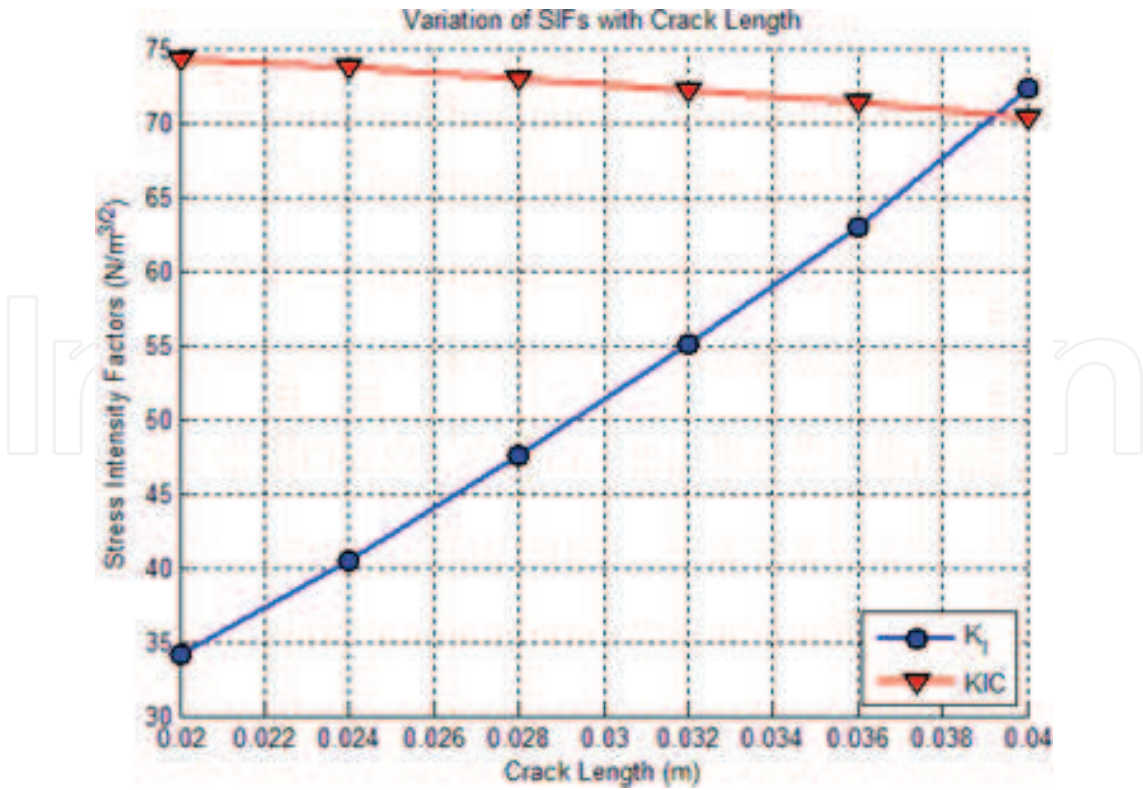


Figure 19. Plot for variation of SIF with crack length for hard inclusions.

## 7. Conclusions

In this chapter we have discussed the simulation of cracks in a FGM plate has been carried out in the presence of multiple inhomogeneities by XFEM using both linear elastic as well as elastic-plastic formulations. SIF has been calculated at the tip of the major crack using interaction integral approach. The variation in the SIF at the tip of the major crack has been studied when multiple inhomogeneities are present in the domain. From this study it is observed that minor cracks have least effect in the FGM plate's failure crack length, whereas soft inclusions have moderate effect and holes have the most severe effect. It is found that the FGM plate's life increases in each case when soft inclusions are replaced by hard inclusions. Hence the presence of the hard inclusions in the plate increases the failure crack length of the plate i.e. plate survives more.

## Nomenclatures

- $\tilde{W}$ : Strain energy  
 $\sigma$ : Stress  
 $\varepsilon$ : Strain  
 $u$ : Deformation  
 $C$ : Compliance matrix  
 $E$ : Modulus of elasticity  
 $\gamma$ : Coefficient of thermal expansion  
 $K_{IC}$ : Critical stress intensity factor (Fracture toughness)

## Author details

Somnath Bhattacharya<sup>1\*</sup>, Kamal Sharma<sup>2</sup> and Vaibhav Sonkar<sup>1</sup>

\*Address all correspondence to: [somnathb.iitr@gmail.com](mailto:somnathb.iitr@gmail.com)

1 Department of Mechanical Engineering, NIT, Raipur, India

2 BARC, Mumbai, India

## References

- [1] Agarwal BD, Kumar P, Khanna SK. Determination of the fracture toughness of fabric reinforced composites by the  $J$ -integral approach. *Composites Science and Technology*. 1986;25:311-323

- [2] Chowdhury SR, Narasimhan R. A finite element analysis of quasi-static crack growth in a pressure sensitive constrained ductile layer. *Engineering Fracture Mechanics*. 2000;**66**:551-571
- [3] Partheepan G, Sehgal DK, Pandey RK. Fracture toughness evaluation using miniature specimen test and neural network. *Computational Materials Science*. 2008;**44**:523-530
- [4] Patil DP, Maiti SK. Detection of multiple cracks using frequency measurements. *Engineering Fracture Mechanics*. 2003;**70**:1553-1572
- [5] Cheung Y, Wang Y, Woo C. A general method for multiple crack problems in a finite plate. *Computational Mechanics*. 1992;**10**:335-343
- [6] Ang WT, Gumel AB. Multiple interacting planar cracks in an anisotropic multilayered medium under an antiplane shear stress: A hypersingular integral approach. *Engineering Analysis with Boundary Elements*. 1996;**18**:297-303
- [7] Denda M, Dong YF. Complex variable approach to the BEM for multiple crack problems. *Computer Methods in Applied Mechanics and Engineering*. 1997;**141**:247-264
- [8] Rice JR. A path independent integral and the approximate analysis of strain concentration by notches and cracks. *Journal of Applied Mechanics*. 1968;**35**:379-386
- [9] Sills BL, Dolev O. The conservative M-integral for thermal-elastic problems. *International Journal of Fracture*. 2004;**125**:149-170
- [10] Choubey A, Sehgal DK, Tandon N. Finite element analysis of vessels to study changes in natural frequencies due to cracks. *International Journal of Pressure Vessels and Piping*. 2006;**83**:181-187
- [11] Khanna SK, Shukla A. Energy absorption mechanisms during dynamic fracturing of fibre-reinforced composites. *Journal of Materials Science*. 1993;**28**:3722-3730
- [12] Zhang J, Yao Z, Tanaka M. The meshless regular hybrid boundary node method for 2-D linear elasticity. *Engineering Analysis with Boundary Elements*. 2003;**27**:259-268
- [13] Zhang J, Yao Z. The regular hybrid boundary node method for three-dimensional linear elasticity. *Engineering Analysis with Boundary Elements*. 2004;**28**:525-534
- [14] Singh IV, Sandeep K, Prakash R. Heat transfer analysis of two-dimensional fins using meshless element-free Galerkin method. *Numerical Heat Transfer: Part A*. 2003;**44**:73-84
- [15] Singh IV, Sandeep K, Prakash R. Application of meshless element free Galerkin method in two-dimensional heat conduction problems. *Computer Assisted Mechanics and Engineering Sciences*. 2004;**11**:265-274
- [16] Rao BN, Rahman S. An efficient meshless method for fracture analysis of cracks. *Computational Mechanics*. 2000;**26**:398-408
- [17] Rao BN, Rahman S. An enriched meshless method for nonlinear fracture mechanics. *International Journal for Numerical Methods in Engineering*. 2004;**59**:197-223
- [18] Bui QT, Nguyen NM, Zhang C. An efficient meshfree method for analysis of two-dimensional piezoelectric structures. *Smart Materials and Structures*. 2011;**20**:065016

- [19] Belytschko T, Black T. Elastic crack growth in finite elements with minimal remeshing. *International Journal for Numerical Methods in Engineering*. 1999;**45**:601-620
- [20] Belytschko T, Parimi C, Moes N, Sukumar N, Usui S. Structured extended finite element methods for solids defined by implicit surfaces. *International Journal for Numerical Methods in Engineering*. 2003;**56**:609-635
- [21] Giudice SD, Comini G, Mikhailov MD. Finite element analysis of combined free and forced convection. *International Journal of Heat Mass Transfer*. 1978;**21**:1619-1621
- [22] Reddy JN, Chao WC. Finite element analysis of laminated bi-modulus composite-material plates. *Computers and Structures*. 1980;**12**:245-251
- [23] Kant T, Menon MP. A finite element-difference computational model for stress analysis of layered composite cylindrical shells. *Finite Elements in Analysis and Design*. 1993;**14**:55-71
- [24] Sze KY, Wang HT. A simple finite element formulation for computing stress singularities at bi-material interfaces. *Finite Elements in Analysis and Design*. 2000;**35**:97-118
- [25] Armentani E, Citarella R. DBEM and FEM analysis on non-linear multiple crack propagation in an aeronautic doubler-skin assembly. *International Journal of Fatigue*. 2006;**28**:598-608
- [26] Yoon JW, Cardoso RPR, Dick RE. Puncture fracture in an aluminum beverage can. *International Journal of Impact Engineering*. 2010;**37**:150-160
- [27] Deodatis G. Stochastic FEM sensitivity analysis for non-linear dynamic problems. *Probabilistic Engineering Mechanics*. 1989;**4**:135-141
- [28] Kant T, Arora CP, Varaiya JH. Finite element transient analysis of composite and sandwich plates based on a refined theory and a mode superposition method. *Composite Structures*. 1992;**22**:109-120
- [29] Yoon JW, Song IS, Yang DY, Chung K, Barlat F. Finite element method for sheet forming based on an anisotropic strain-rate potential and the convected coordinate system. *International Journal of Mechanical Science*. 1995;**37**:733-752
- [30] Yoon JW, Yang DY, Chung K. Elasto-plastic finite element method based on incremental deformation theory and continuum based shell elements for planar anisotropic sheet materials. *Computer Methods in Applied Mechanics and Engineering*. 1999;**174**:23-56
- [31] Andreev K, Harmuth H. FEM simulation of the thermo-mechanical behaviour and failure of refractories-a case study. *Journal of Materials Processing Technology*. 2003;**143-144**:72-77
- [32] Huang ZM. Failure analysis of laminated structures by FEM based on nonlinear constitutive relationship. *Composite Structures*. 2007;**77**:270-279
- [33] Dias AMPG, Kuilen JWVD, Lopes S, Cruz H. A non-linear 3D FEM model to simulate timber-concrete joints. *Advances in Engineering Software*. 2007;**38**:522-530
- [34] Coda HB. A solid-like FEM for geometrically non-linear 3D frames. *Computer Methods in Applied Mechanics and Engineering*. 2009;**198**:3712-3722

- [35] Bhattacharya S, Singh IV, Mishra BK. Mixed-mode fatigue crack growth analysis of functionally graded materials by XFEM. *International Journal of Fracture*. 2013;**183**:81-97
- [36] Yu H, Wu L, Guo L, He Q, Du S. Interaction integral method for the interfacial fracture problems of two non-homogeneous materials. *Mechanics of Materials*. 2010;**42**:435-450
- [37] Sukumar N, Prevost J. Modeling quasi-static crack growth with the extended finite element method part I: Computer implementation. *International Journal of Solids and Structures*. 2003;**40**:7513-7537
- [38] Arola D, Huang MP, Sultan MB. The failure of amalgam dental restorations due to cyclic fatigue crack growth. *Journal of Materials Science: Materials in Medicine*. 1999;**10**:319-327
- [39] Roylance D. *Fatigue*, Department of Materials Science and Engineering, Cambridge: Massachusetts Institute of Technology. 2001;Vol. 02139
- [40] Hsieh CL, Tuang WH. Poisson's ratio of two phase composites. *Materials Science and Engineering A*. 2005;**396**:202-205
- [41] Raveendran KV, Vermam AP, Rao CVSK. Effective fracture toughness of composites. *International Journal of Fracture*. 1991;**47**:63-65
- [42] Shedbale AS, Singh IV, Mishra BK. Nonlinear simulation of an embedded crack in the presence of holes and inclusions by XFEM. *Procedia Engineering*. 2013;**64**:642-651
- [43] Bhattacharya S, Sharma K, Sonkar V. Numerical simulation of elastic plastic fatigue crack growth in functionally graded material using the extended finite element method. *Mechanics of Advanced Materials and Structures*. 2017 <http://dx.doi.org/10.1080/15376494.2016.1227511>
- [44] Bhattacharya S, Singh IV, Mishra BK, Bui TQ. Fatigue crack growth simulations of interfacial cracks in bi-layered FGMs using XFEM. *Computational Mechanics*. 2013b;**52**:799-814